The Astrophysical Journal, 789:2 (10pp), 2014 July 1 doi:10.1088/0004-637X/789/1/2

THEORETICAL HOT METHANE LINE LISTS UP TO $T = 2000$ K FOR ASTROPHYSICAL APPLICATIONS

M. Rey[1], A. V. Nikitin[2,3], and Vl. G. Tyuterev[1]
[1] Groupe de Spectrométrie Moléculaire et Atmosphérique, UMR CNRS 7331, BP 1039, F-51687, Reims Cedex 2, France; michael.rey@univ-reims.fr
[2] Laboratory of Theoretical Spectroscopy, Institute of Atmospheric Optics, SB RAS, 634055 Tomsk, Russia
[3] Tomsk State University, 36 Lenin Avenue, 634050 Tomsk, Russia
Received 2013 December 16; accepted 2014 April 27; published 2014 June 9

ABSTRACT

The paper describes the construction of complete sets of hot methane lines based on accurate ab initio potential and dipole moment surfaces and extensive first-principle calculations. Four line lists spanning the [0–5000] cm^{-1} infrared region were built at $T = 500$, 1000, 1500, and 2000 K. For each of these four temperatures, we have constructed two versions of line lists: a version for high-resolution applications containing strong and medium lines and a full version appropriate for low-resolution opacity calculations. A comparison with available empirical databases is discussed in detail for both cold and hot bands giving a very good agreement for line positions, typically <0.1–0.5 cm^{-1} and $\sim 5\%$ for intensities of strong lines. Together with numerical tests using various basis sets, this confirms the computational convergence of our results for the most important lines, which is the major issue for theoretical spectra predictions. We showed that transitions with lower state energies up to 14,000 cm^{-1} could give significant contributions to the methane opacity and have to be systematically taken into account. Our list at 2000 K calculated up to $J = 50$ contains 11.5 billion transitions for $I > 10^{-29}$ cm mol^{-1}. These new lists are expected to be quantitatively accurate with respect to the precision of available and currently planned observations of astrophysical objects with improved spectral resolution.

Key words: brown dwarfs – infrared: general – methods: numerical – molecular data

Online-only material: color figures, machine-readable table, supplemental data

1. INTRODUCTION

Methane (CH_4) is the second strongest absorber after water in near-infrared (NIR) spectra and plays a central role in the radiative transfer and in the physical chemistry for various astrophysical objects with large ranges of effective temperatures $T_{\rm eff}$: from 80 K for giant planets or Titan's atmosphere (Nixon et al. 2012) up to around 3000 K for brown T/L dwarfs (Leggett et al. 2007; Nakajima et al. 2001; Oppenheimer et al. 1995).

Knowledge of intensities of rovibrational transitions of methane in a wide spectral range is thus essential for the modeling of various planetary atmospheres, brown dwarfs, and for other astrophysical applications (Tinetti et al. 2007b; Swain et al. 2010; Hargreaves et al. 2012). This demonstrates the necessity of having adequate and reliable molecular line lists to satisfy these demands. NIR spectra of T dwarfs clearly show the presence of methane, which is the characteristic absorber (consequently referred to as *methane dwarfs*), as well as strong water bands and collision-induced H_2. Moreover, the observation of Gliese 229B (Nakajima et al. 1995) has shown that the NIR spectrum is dominated by strong absorption bands of methane at 1.7, 2.4, and 3.3 μm. In particular, the strong band of methane around 3 μm completely dominates the spectrum of brown dwarfs at 1600 K and is still identifiable at 1800 K (Borysov et al. 2002). Until recently, such broad absorption bands were only found in the giant planets of the solar system and in Titan's atmosphere and significantly modify the NIR broadband colors. Although NIR spectra of L dwarfs show strong absorption bands of water and CO, it has been suggested that methane is present in absorption in the H- and K-band spectra of 2M 0920+35 (Nakajima et al. 2001). Indeed, methane is expected to be present in the lower-temperature upper reaches of the L-dwarf atmosphere, and the 3.3 μm band in the pentad region has been observed even in mid-type L dwarfs (Noll et al. 2000). The L/T-type brown dwarf transition is also determined by the appearance of methane that gradually forms at the expense of CO between $T_{\rm eff} = 1800$ and 1000 K.

The infrared range is ideal for probing the neutral atmospheres of exoplanets; the spectral features being more intense than in the visible (Tinetti et al. 2007a). A recent analysis of observations of the hot Neptune GJ436b suggested that methane is the dominant absorber in this atmosphere (Beaulieu et al. 2011). Methane spectral signatures have also been observed in atmospheres of many other exoplanets (Swain et al. 2008, 2009, 2010; Moses et al. 2011). The number of discovered exoplanets has grown by three orders of magnitude during the last two decades (Tinetti et al. 2013). To analyze these objects, atmospheric models of exoplanets have been developed, making the need again for better spectroscopic data crucial for their interpretation. The upper atmosphere of an exoplanet can be efficiently probed by transit technique and transmission spectroscopy (Coustenis et al. 2006), which is an excellent diagnostic tool to understand the physical chemistry under extreme temperature conditions (Tinetti et al. 2013). However, well-known spectroscopic databases for methane, such as HITRAN/TDS/STDS/MeCaSDa (see Rothman et al. 2013; Ba et al. 2013, and references therein), are mostly based on line-by-line analyses of room-T and low-T spectra. Information on so-called hot bands (HBs) associated with transitions from/to rovibrational patterns of highly excited vibrational states is thus missing or very insufficient for the astrophysical applications cited above. High-T laboratory methane spectra have been recorded, e.g., see Nassar & Bernath (2003), Thiévin et al. (2008), and Hargreaves et al. (2012), who have provided thousands of new lines, but their full analyses have not yet been accomplished. Many observed transitions were not assigned for lower or upper energies. Line-by-line intensity determinations in extremely dense high-T emission spectra that contain

millions of overlapping lines in the conditions of possible temperature gradients and self-absorption effects are excessively complicated, at least without reliable theoretical predictions. Increasing computer power and improvement of the methods for molecular quantum chemistry calculations have made possible quite reliable ab initio spectra predictions at high-T conditions. Successful examples for astrophysical applications are large range hot water spectra predictions by Partridge & Schwenke (1997) and Barber et al. (2006) and more recent calculations for ammonia (Yurchenko et al. 2011; Huang et al. 2011). Hot spectra calculations for some molecules have been assembled in HITEMP (Rothman et al. 2010) and ExoMol (Tennyson & Yurchenko 2012) databases. In the case of methane, the first published theoretical line list was that of Warmbier et al. (2009) at $T = 1000$ K, which was a significant step forward in the understanding of temperature effects. They have argued that radiative transport calculations used to model stellar and planetary atmospheres need complete and consistent spectroscopic high-T databases. This is to avoid incomplete microphysics and thus systematic errors in the determination of atmospheric profiles and other macroparameters. Because high-resolution ab initio spectra prediction for five atomics is a very challenging task, they have made several approximations (classical treatment of rotational energies, state averaging, etc.). They also stated that the exact quantum mechanical calculation for $J > 0$ at that time was not possible, and that their calculation "does not have a quantitative message, but provides a proof of principle" for the approach. In this paper, we briefly outline the advances in methane theoretical spectra predictions that now allow full quantum-mechanical quantitatively accurate ab initio calculations for energies, line positions, and intensities (see Section 2). Based on the progress in computational methods, we have constructed here for the first time theoretical methane line lists up to $T = 2000$ K for astrophysical applications. Our calculations account in a consistent way for most accurate available potential energy, for dipole moment ab initio surfaces, and for molecular symmetry properties (see Section 3). Comparisons with the HITRAN database as well as with existing cold and hot T experimental laboratory spectra by Hargreaves et al. (2012, 2013) allow for the validation of the quantitative accuracy of our new line lists (see Section 4). The temperature effects and related issues for astrophysical applications are discussed in Section 5.

2. STATE OF THE ART IN METHANE SPECTROSCOPY: LABORATORY MEASUREMENTS AND CALCULATIONS

Infrared methane spectra are known to be quite complex primarily because of the high molecular symmetry of CH_4. This gives rise to degeneracies and quasi-degeneracies of the vibration modes and to vast and complicated resonance interactions due to inter-mode couplings. The four normal mode frequencies of methane exhibit an approximate relation between stretching and bending frequencies with $\omega_1 \approx \omega_3 \approx 2\omega_2 \approx 2\omega_4 \approx 3000$ cm^{-1} resulting in vibrational levels grouped into polyads with levels of nearby energies. Each polyad P_n is defined by the integer polyad number $n = 2(v_1 + v_3) + v_2 + v_4$, where (v_1, v_2, v_3, v_4) are principal vibrational normal mode quantum numbers taking values 0, 1, 2, etc. The ground state (GS) polyad (P_0) contains only the (0000) vibrational state, the dyad (P_1) contains {(0100)/(0001)} with the rovibrational levels in the energy range $E/hc > 1310$ cm^{-1}, the pentad (P_2) contains {(1000)/(0010)/(0200)/(0101)/(0002)} in the energy range $E/hc > 2587$ cm^{-1}, and so on. As the ν_2 mode is doubly degenerate and ν_3 and ν_4 are triply degenerate, the overtone and combination vibrational levels contain vibrational sublevels whose number rapidly increases with the vibration excitation. The octad (P_3) with $E/hc > 3870$ cm^{-1} contains 8 vibrational levels with 24 sublevels. The following polyad is the tetradecad (P_4) with $E/hc > 5122$ cm^{-1} (14 levels, 60 sublevels), while the highest polyads P_9 (heptacontad) accounted for in our new line list contains 70 vibrational levels with 1746 sublevels. Overlapping among rovibrational patterns of various vibrational sublevels result in dense polyad structures that are very difficult to analyze. Their complexity drastically increases with the rotational quantum number J.

Much effort has been recently devoted to extend laboratory measurements of methane spectra using Fourier transform (Albert et al. 2009) with long optical path cell (Nikitin et al. 2011a) and using laser techniques (Campargue et al. 2013) as recently reviewed by Brown et al. (2013, and references therein). Most of available experimental spectra have been recorded at room or at cold temperatures for atmospheric applications. Even at these conditions, line-by-line analyses of crowded methane spectra are tedious. In order to account for the high tetrahedral symmetry of methane, a symmetry-adapted formalism has been developed and implemented for effective polyad models in Dijon, Tomsk, and Reims groups (Champion 1977; Boudon et al. 2004; Nikitin et al. 2012). This line-by-line approach that relies on empirical fits of a large number of effective spectroscopic parameters with successive extrapolations can only progress slowly by considering one polyad after the other. Over the past 30 years, about 21,400 lines of $^{12}CH_4$ *cold bands* (CB) corresponding to P_i–P_0 transitions up to $i = 5$ have been assigned, and 10,100 measured line intensities have been included in empirical models (Brown et al. 2013). This results in good knowledge of rovibrational energy levels up to P_3 with moderate values of rotational quantum numbers ($J < 20$). For P_4, only about 25% of sublevels have been explored in analyses of experimental spectra, and for P_5, only few low-edge bands have been analyzed (Nikitin et al. 2011c, 2013a). Considerable progress in CB measurements and analyses has resulted in a significant improvement of the modeling of Titan's atmosphere (de Bergh et al. 2012; Hirtzig et al. 2013) for which IR opacity is dominated by methane absorption. However, many of experimental methane spectra, in particular for higher polyads, remain unassigned. The HITRAN database (Rothman et al. 2009, 2013) assembles up-to-date measured lines, as well as those extrapolated from empirical effective models, but information on hot bands HBs is very limited: only P_2–P_1 and P_1–P_1 line-by-line analyses of experimental intensities are available in HITRAN2008 while no new HB analyses were published between the HITRAN2008 and HITRAN2012 versions. Experimental laboratory studies of high-T methane spectra are still quite seldom. A significant step forward has been achieved by Nassar & Bernath (2003) and by Thiévin et al. (2008), who recorded experimental methane cross sections up to 6400 cm^{-1} and temperatures up to 1800 K around 3 μm. Recently, experimental line lists of hot CH_4, hereafter denoted as HBMIB, have been built by Hargreaves et al. (2012, 2013) from a dozen hot emission spectra up to 1673 K and in the range 2–10.4 μm (Hargreaves et al. 2012, 2013). Consequently, lower state energies E_{low} were estimated empirically—but not systematically—from the Boltzmann statistics and intercomparisons of spectra at different temperatures.

On the theoretical side, significant progress has been recently achieved in ab initio spectra predictions. These calculations

Table 1
Convergence of the Integrated Intensity ($\sum S_{ij}$)$_{\rm theo}$ (in cm mol^{-1}) as a Function of $J_{\rm max}$ and $E_{\rm low,max}$ (in cm^{-1}) in Our Variational Calculations

	500 K	1000 K	1500 K	2000 K
	($\times 10^{-17}$ cm mol^{-1})	($\times 10^{-17}$ cm mol^{-1})	($\times 10^{-17}$ cm mol^{-1})	($\times 10^{-17}$ cm mol^{-1})
$J \leqslant 10$	1.199	0.667	0.416	0.255
$J \leqslant 20$	1.795	1.669	1.353	0.936
$J \leqslant 30$	1.805	1.846	1.734	1.368
$J \leqslant 40$	1.805	1.852	1.779	1.456
$J \leqslant 50$	1.805	1.852	1.781	1.462
$E_{\rm low} \leqslant 5000$	1.805	1.686	1.031	...
$E_{\rm low} \leqslant 8000$	1.805	1.842	1.593	1.063
$E_{\rm low} \leqslant 11000$	1.805	1.852	1.767	1.403
$E_{\rm low} \leqslant 14000$	1.805	1.852	1.781	1.462

Notes. Intensity cutoff was fixed to $I_{\rm cutoff} = 10^{-27}$, 10^{-28}, 10^{-29}, and 10^{-29} for $T = 500$, 1000, 1500, and 2000 K.

require potential energy surface (PES) to quantify nuclear motions and to compute rovibrational energy levels and line positions. Schwenke & Partridge (2001) investigated the role of various approximations in electronic structure PES calculations, which were used by Wang & Carrington (2003) to study a convergence of vibration–rotation calculations. At the second step, line intensities are to be computed using dipole moment surface (DMS). Cassam-Chenai & Liévin (2012) calculated in this way intensities for rotational $P_0 \rightarrow P_0$ transitions, while Yurchenko et al. (2013) estimated vibrational band strengths in the IR range. The most accurate up-to-date methane PES and DMS were recently reported by Nikitin et al. (2011b, 2013b). For the rotational transitions, this allowed an average calculation accuracy of $\sim 10^{-3}$ cm^{-1} up to $J = 17$ (Tyuterev et al. 2013), while for band centers observed at room T, the rms deviation between theory and experiment was 0.08, 0.25, and ~ 1 cm^{-1} up to the pentad, octad, and tetradecad, respectively. Drastic improvements also have been achieved from first-principle line intensity predictions at room and low temperatures in a large IR wavenumber range of 0–9300 cm^{-1}. For integrated CB intensities at $T = 300$ K with $J_{\rm max} = 20$, the agreement between our previous ab initio calculations and observations was 4% for dyad (P_1–P_0), 2.5% for pentad (P_2–P_0), 1.5% for octad (P_3–P_0), 6% for tetradecad (P_4–P_0), 3% for icosad (P_5–P_0), and about 5% for triacontad (P_6–P_0) transitions, as reported by Nikitin et al. (2013b) and Rey et al. (2013a, 2013b).

3. COMPUTATIONAL METHODS

In this work, we extend our theoretical predictions for methane absorption/emission lines to high temperatures ($T \sim 2000$ K) that are relevant for astrophysical applications. The aim is a construction of complete line lists accounting for all HB transitions which could contribute to the absorption or emission at these extreme conditions with a subsequent validation against available high-resolution experimental spectra. The line-by-line computational method is based on full quantum-mechanical calculations. Infrared line intensities $S_{\rm if}$ of rovibrational transitions $\nu_{\rm if}$ for a given temperature T are defined in HITRAN units (cm^{-1}/(molecule cm^{-2}) and simply denoted as cm molecule^{-1} in the following) as

$$S_{\rm if} = \frac{8\pi^3 10^{-36}}{3hcQ(T)} g_{C_i} \nu_{\rm if} e^{-c_2 E_i/T} (1 - e^{-c_2 \nu_{\rm if}/T}) \mathcal{R}_{\rm if}, \qquad (1)$$

where $c_2 = hc/k$, g_{C_i} and E_i are the nuclear spin statistical weight and the energy of the lower state. $Q(T)$ is the partition function and $\mathcal{R}_{\rm if}$ is the square transition-moment matrix. At this stage, three major theoretical "ingredients" are necessary.

1. An accurate intra-molecular PES at a large range of vibrational displacements is to be used to predict rovibrational energy levels E_i and line positions ν_{ij}.
2. DMS components μ also defined in a large range of nuclear configurations are necessary for calculation of transition probabilities between upper and lower vibration–rotation states.
3. Efficient computational methods are required to account for molecular symmetry properties and to achieve a good numerical convergence of calculations in a large basis set.

For steps 1 and 2, we use nine-dimensional methane surfaces developed in our previous works (Nikitin et al. 2011b, 2013b), which will hereafter be referred to as Nikitin–Rey–Tyuterev (NRT) PES and DMS. As mentioned in the previous section, the use of these surfaces has allowed significant improvement of calculations for low- and room-temperature spectra. For step 3, we use the variational approach with a full account of the high T_d symmetry of methane. Extension to high-T predictions is quite a challenge as higher polyads and higher J states are populated (Figure 1 and Table 1). The major issue is to minimize the cost of computations and the loss of accuracy in all calculations. To this end, we employ a truncation–compression technique using normal coordinates as described in our previous works (Rey et al. 2012, 2013a). Note that spectra predictions for isotopic ^{12}C/^{13}C and H/D substitutions were also reported (Rey et al. 2013a, 2013b).

The results for energies obtained from the same PES were checked by three different computational methods. We have previously computed CB centers in internal non-rectilinear coordinates without power series PES expansions, using the exact kinetic energy operator (Nikitin et al. 2011b) giving an average agreement with our normal mode calculations better than 0.1 cm^{-1} up to the tetradecad range. The validity of our rotational and vibrational methane calculations also have been confirmed by an independent algebraic approach (contact transformation method), which gave an rms deviation of 0.76 cm^{-1} with available experimental values for the centers of all presently analyzed bands of $^{12}CH_4$ up to the triacontad range of 0–9000 cm^{-1} (Tyuterev et al. 2013). Note that accurate predictions of energies and thus line positions, could be important even for low-resolution spectra because of intensity transfers between strong and weak bands. The validity of line intensity calculations was checked using two program suites: TENSOR code (Rey et al. 2013a) and MIRS code (Nikitin et al. 2012), the latter one being

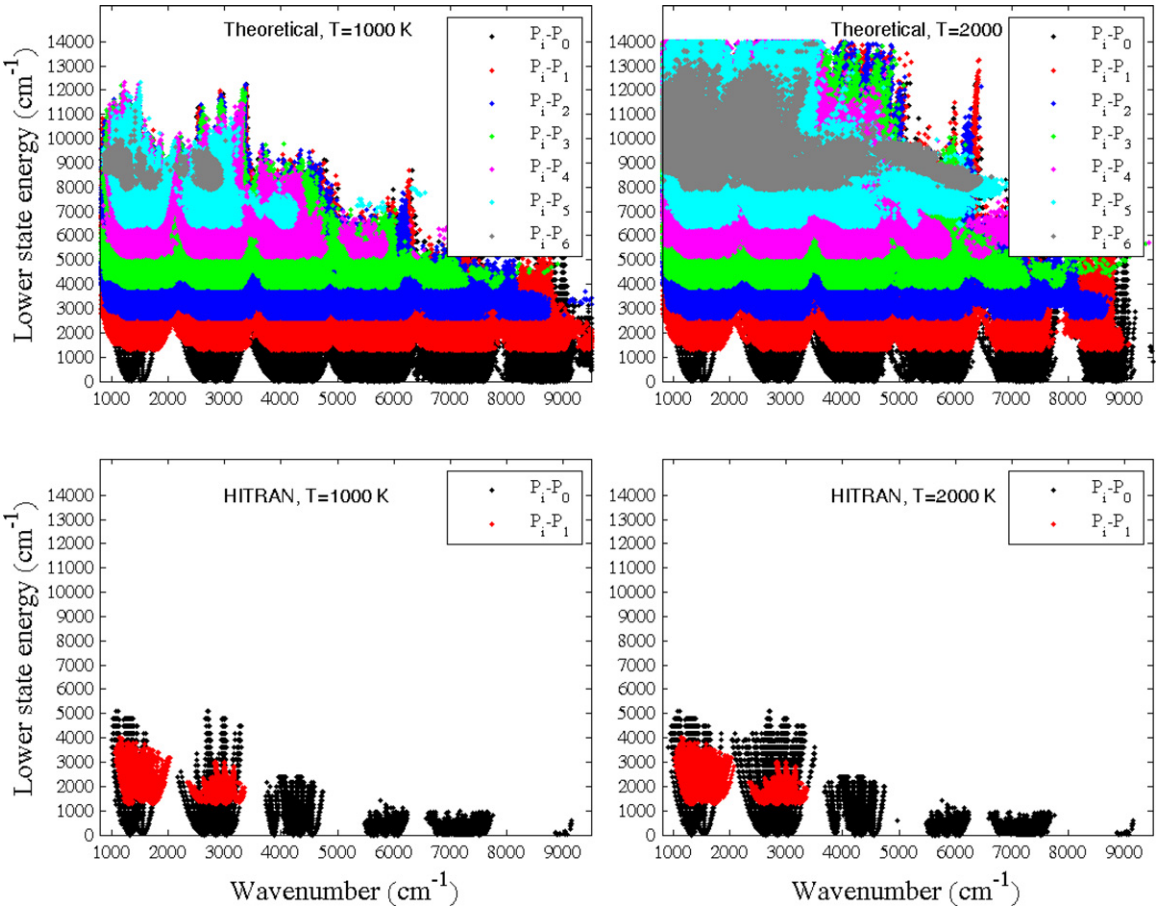

Figure 1. Comparison of the lower state energies involved in the database transitions between theoretical predictions (this work; top panel) and HITRAN 2008 (bottom panel). The intensity cutoff was fixed to 5×10^{-27} cm mol^{-1}. Qualitative predictions above 5000 cm^{-1} are also given. Each color represents P_i–P_j CBs and HBs. (A color version of this figure is available in the online journal.)

previously validated by experimental spectrum analyses using effective spectroscopic models.

Both PES and DMS surfaces are treated here in a consistent way using the same method of quantum chemistry (coupled clusters method) with a very similar choice of electronic orbitals included and modeled with the same choice of analytical expansions. We did not use any rotor approximations: both anharmonic and Coriolis vibration–rotation couplings were considered in line position and line intensity calculations.

4. RESULTS: THEORETICAL HIGH-TEMPERATURE METHANE LINE LISTS

From the NRT PES, we first computed the rovibrational energy levels for $J \leqslant 50$ and estimated the partition function given by $Q(T) = \sum(2J+1)g_C\exp(-c_2E_{vJ}/T)$. The values obtained at different temperatures are given in Table 2 and are in quite good agreement with the literature. Using the approach described above, we have generated a theoretical database covering the far- and near-infrared range for $^{12}CH_4$. This database was built up to 2000 K for $J \leqslant 50$ by including strong, medium, and weaker lines up to 5000 cm^{-1}. To be consistent and nearly complete at 2000 K, our list was generated by taking the lower state energy cutoff as $E_{\rm low,max} = 14{,}000$ cm^{-1} (see Figure 1). The choice for this value is twofold: it avoids that some upper states probe potential regions where the PES representation could not be sufficiently reliable, and it allows computing P_3–P_0 transitions (octad region) up to $J = 45$, and thus fixes the effective spectral range as [0–5000] cm^{-1}.

Table 2
Methane Partition Function Calculated from Variational Rovibrational Energy Levels

T (K)	This Work	HITRAN	Wenger et al. (2008)
296	590.49	590.44 (0%)	590.50 (0%)
500	1417.54	1417.7 (0%)	1417.7 (0%)
1000	8065.32	7980.7 (1%)	8067.4 (0.02%)
1500	40081.73	39195.5 (2.2%)	40577.0 (1.2%)
2000	165270.0	168386.0 (1.7%)	191000.0 (13%)

Notes. Comparisons with HITRAN and Wenger et al. (2008) are also given with corresponding descrepancies from this work in parentheses.

(This table is available in its entirety in a machine-readable form in the online journal. A portion is shown here for guidance regarding its form and content.)

For each of the four temperatures, we have constructed two versions of line lists. The "full" version contains all transitions up to $J = 50$, including a tremendous number of very weak lines which are necessary to account for opacity calculations in the case of low-resolution remote sensing observations. In the case of $T = 2000$ K, the list contains 11.5 billion transitions for $I > 10^{-29}$ cm mol^{-1}. Most of these tiny transitions could not be visible as individual lines because of their very high density, which increases rapidly with T as shown in Figures 2 and 3. The accuracy of the predictions obviously deteriorates with increasing energies and with decreasing intensity cutoffs. However, the errors in very weak transitions are less important

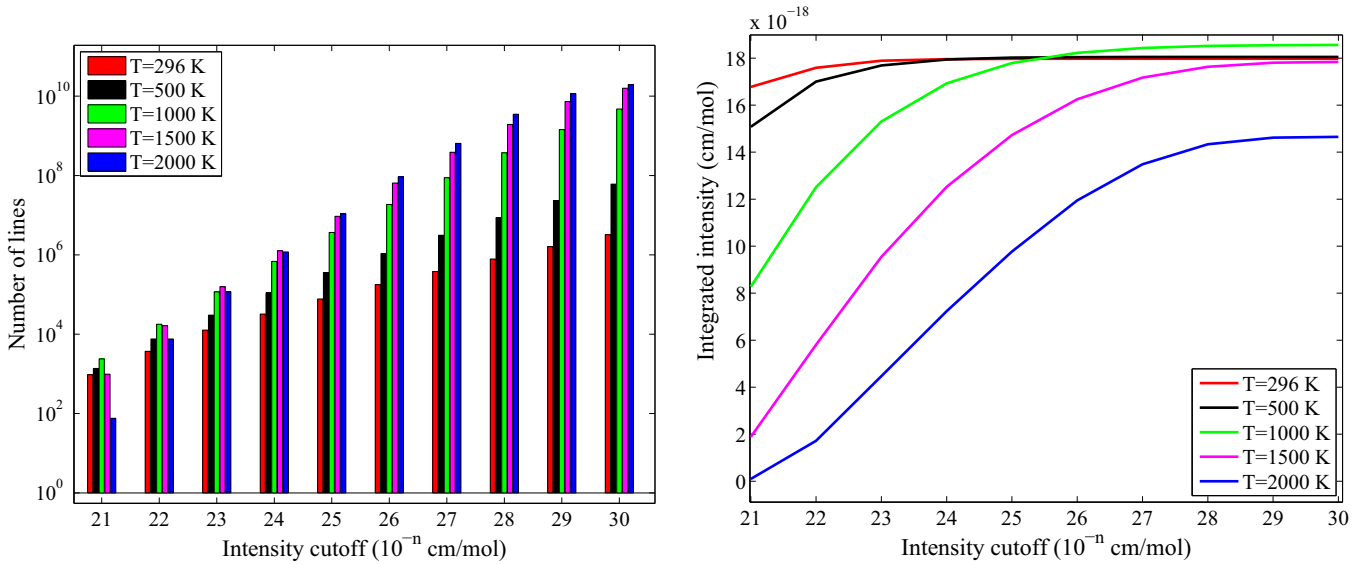

Figure 2. Number of lines (left panel) and convergence of the integrated intensity (in cm mol^{-1}; right panel) as a function of the intensity cutoff for different temperatures.

(A color version and supplemental data for this figure are available in the online journal.)

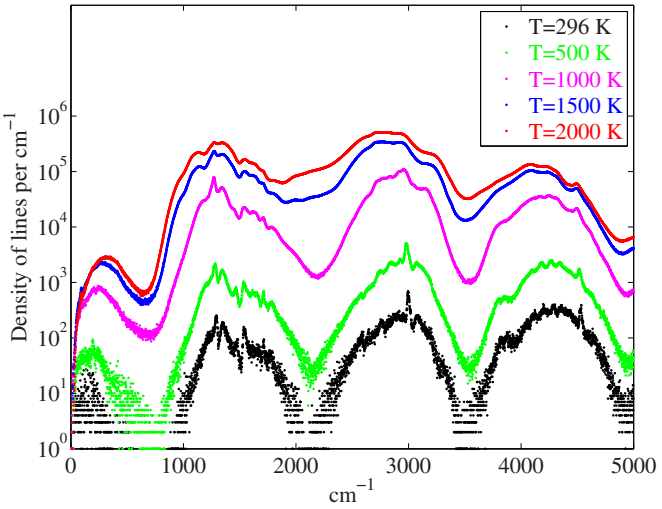

Figure 3. Density of lines per cm^{-1} for our lists with intensities $>10^{-27}$ cm mol^{-1} for different temperatures.

(A color version of this figure is available in the online journal.)

Table 3
Accuracy of Our Room-temperature Predictions ($T = 296$ K) in the Range [0–5000] cm^{-1} Compared to HITRAN for the Rotational Dependence of Line Positions and for Intensities

I_{cutoff}	CB/HB	Lines	rms (cm^{-1})	rms (%)
cm molecules^{-1}			Positions[a]	Intensities
10^{-23}	CB	7912	0.057	4.1
	HB	863	0.016	1.0
10^{-24}	CB	14810	0.070	4.8
	HB	2335	0.026	1.3
10^{-25}	CB	21556	0.087	4.8
	HB	5585	0.039	2.2
10^{-26}	CB	27493	0.10	5.1
	HB	10119	0.06	3.1

Notes. Errors were estimated from extracted theoretical lines corresponding to the same assignments as those given in HITRAN2008 at different intensity cutoffs.

[a] Vibrational ($J = 0$) band centers were matched to experimental values using the vibrational sub-space approach as described by Rey et al. (2013a).

for applications since their contributions are averaged within a kind of quasi-continuum in the absorption/emission spectra. An illustrative example, Figure 3 gives the density of lines per cm^{-1} for $I_{cutoff} = 10^{-27}$ for all temperatures. At 2000 K, we see that the density can reach up to 10^6 lines per cm^{-1}; this value being higher than the entire set of available experimental databases. The recent observed data require a good estimation of the methane opacity. In order to model and describe the methane spectra in a proper way, we have systematically studied, for a given T, the convergence of the integrated line intensities with respect (1) to the global intensity cutoff I_{cutoff} in the range of 10^{-21}–10^{-30} cm mol^{-1} up to $T = 2000$ K and (2) to HB and polyad contributions. For $T = 2000$ K, it turns out that P_{i+j}–P_j HBs with $j = 0, \cdots, 6$ contributes significantly to the methane opacity. Though weak transitions are not observable as isolated lines in laboratory experiments, intensities of about 10^{-29}–10^{-30} cm mol^{-1} have to be included to converge the sum of strength and thus have an impact on low-resolution spectra for opacity calculations. Figure 2 illustrates the convergence of the integrated intensity as a function of I_{cutoff} for different temperatures. We also give in Figure 2 the number of lines from room T to 2000 K as I_{cutoff} decreases. All the detailed results and statistics for each polyad and temperature are available in the online journal. For each temperature, we are thus able to determine the appropriate cutoff for building the line lists without loss of opacity. The integrated intensities are fully converged for $I_{cutoff} = 10^{-26}$, 10^{-27}, 10^{-28}, 10^{-29}, and 10^{-29} cm mol^{-1} at $T = 296$, 500, 1000, 1500, and 2000 K, respectively. The corresponding line lists are composed of 3 million, 337 million, 7 billion, and 11.5 billion lines at $T = 500$ K, 1000 K, 1500 K, and 2000 K. Table 1 illustrates the convergence of the integrated intensities as a function of J_{max} and $E_{low,max}$ and proves that for $J \leqslant 50$ and $E_{low} \leqslant 14{,}000$ cm^{-1} our lists are nearly complete. Note that for intensity $>10^{-30}$ cm mol^{-1}, the list would contain nearly 20 billion lines at 2000 K, but would bring only 0.2% of additional

Table 4
Line List Summary at $T = 500$, 1000, 1500, and 2000 K, and Comparisons with HITRAN Extrapolated at the Corresponding Temperatures and with ExoMol in the Range of [0–5000] cm^{-1}

	Theoretical (This Work)		HITRAN2008	Theoretical ExoMol
	$(\sum S_{ij})_{theo}$		$(\sum S_{ij})_{HITRAN}$	$(\sum S_{ij})_{10to10}$
$T = 500$ K	1.81×10^{-17} ($I > 10^{-27}$)		1.74×10^{-17}	1.79×10^{-17}
$T = 1000$ K	1.85×10^{-17} ($I > 10^{-28}$)		1.17×10^{-17}	1.83×10^{-17}
$T = 1500$ K	1.78×10^{-17} ($I > 10^{-29}$)		4.56×10^{-18}	1.61×10^{-17}
$T = 2000$ K	1.46×10^{-17} ($I > 10^{-29}$)		1.39×10^{-18}	1.08×10^{-17}[a]
	N Lines	%	N Lines	N Lines
$T = 500$ K				
P_i–P_0	187,387	89.8	68,673	184,798
P_i–P_1	893,562	9.5	40,498	923,230
P_i–P_2	1,424,701	0.7	4735	1,591,725
P_i–P_3	575,360	0.04		696,652
P_i–P_4	45,680	8×10^{-6}		32,987
P_i–P_5	174	≈0		165
P_i–P_6	0	0		0
⇒	**3,126,864**		**113,906**	**3,429,557**
$T = 1000$ K				
P_i–P_0	580,603	41.6	81,310	522,207
P_i–P_1	4,721,104	31.2	44,827	4,445,188
P_i–P_2	23,291,962	16.9	16,682	22,974,349
P_i–P_3	70,315,137	7.1		68,127,336
P_i–P_4	127,582,629	2.5		115,196,073
P_i–P_5	120,528,292	0.7		72,899,755
P_i–P_6	27,059,113	0.06		850,621
⇒	**374,078,840**		**142,819**	**285,015,529**
$T = 1500$ K				
P_i–P_0	1,115,367	14.9	72,563	725,323
P_i–P_1	11,319,151	21.5	41,603	7,032,011
P_i–P_2	74,787,195	22.8	13,806	42,959,313
P_i–P_3	330,169,127	18.5		155,480,723
P_i–P_4	1,124,558,425	12.9		350,961,956
P_i–P_5	2,664,128,626	7.2		331,081,460
P_i–P_6	3,120,351,384	2.0		4,775,728
⇒	**7,326,429,275**		**127,972**	**893,016,514**
$T = 2000$ K				
P_i–P_0	1,211,275	6.3	69,231	720,081
P_i–P_1	13,085,709	12.5	36,495	7,003,033
P_i–P_2	92,359,447	18.6	7808	43,122,498
P_i–P_3	425,090,999	21.0		157,962,372
P_i–P_4	1,575,646,030	20.3		362,796,507
P_i–P_5	3,870,288,224	15.4		350,453,827
P_i–P_6	5,565,730,599	5.9		5,198,279
⇒	**11,543,412,283**		**113,534**	**927,256,597**

Notes. HITRAN intensities were renormalized by dividing by the isotopic abundance 0.9882. $\sum S_{ij}$ (in cm mol^{-1}) is the integrated intensity and (%) is the intensity contribution with respect to $(\sum S_{ij})_{theo}$.
[a] Extrapolation to $T = 2000$ K from the $T = 1500$ K list of Yurchenko & Tennyson (2014). N = number of lines by polyad calculated with the same intensity cutoff for both lists. The total number of lines for a given T in the lists is given in bold.

opacity in the full range of 0–5000 cm^{-1}. In the pentad region around 3 μm, our line lists are complete and contain CB and HB P_2–P_0, P_3–P_1, P_4–P_2, P_5–P_3, P_6–P_4, P_7–P_5, and P_8–P_6 transitions. The highest polyad considered in our line lists is P_9, which is involved in P_9–P_6 HBs around 2.5 μm. Our lists contain (ν_{if} (cm^{-1}), S_{if} (cm $molecule^{-1}$), E_{low} (cm^{-1}))[4]. The lists with intermediate T could be built from Equation (1) and the table of $Q(T)$ in the online journal. In Table 4, we have summarized the four lists, and all the detailed contributions of CBs and HBs are given. As expected, HBs predominate as T increases and a fortiori lead to very dense and complex spectra. This table also gives the integrated intensities in the range of [0–5000] cm^{-1}. We thus see that for $T = 500$ K, most of the line intensity contributions come from cold P_i–P_0 bands, while for $T > 1500$ K, they represent less than 20%. This means that for high-temperature applications, HBs prove to be of great importance from $T = 500$ K.

For high-resolution applications and for rotational assignments of laboratory spectra, we also provide "light" versions of our lists that contain relatively strong and medium lines. The

[4] Our list are available at http://vamdc.univ-reims.fr/nas/.

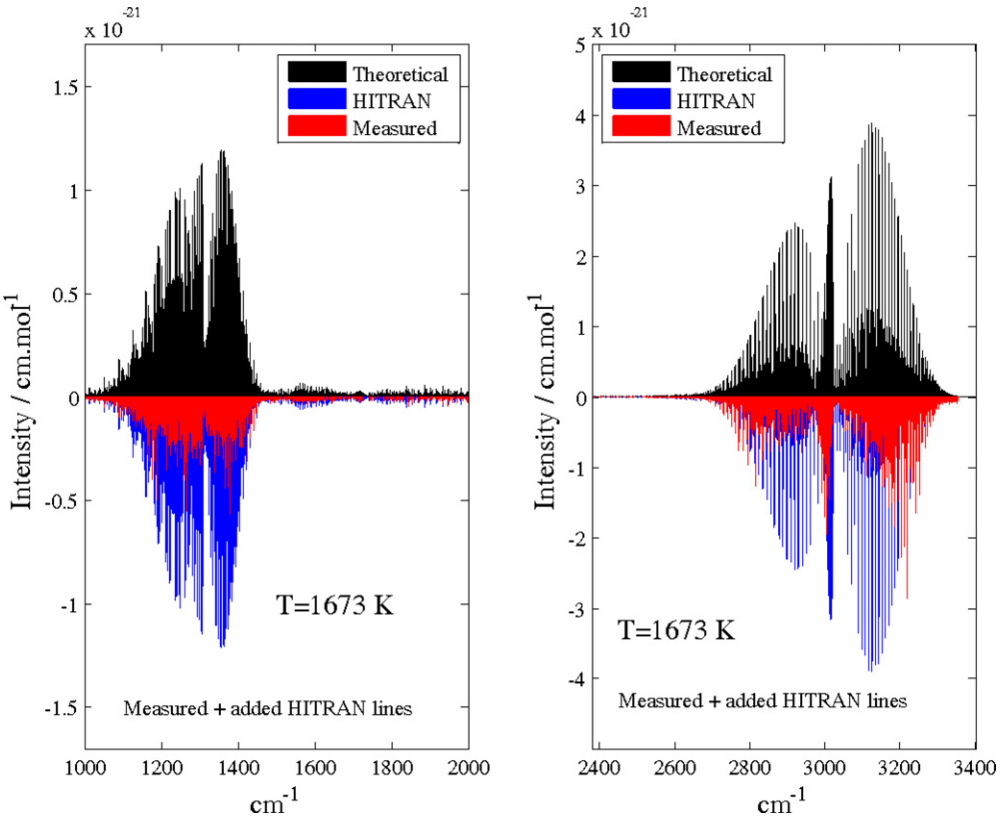

Figure 4. Comparison of the stick spectrum of the dyad (left panel) and pentad (right panel) between the theoretical calculations (this work) and the experimental line list at 1673 K by Hargreaves et al. (2012, 2013). The latter is composed by measured lines combined with HITRAN lines.

(A color version of this figure is available in the online journal.)

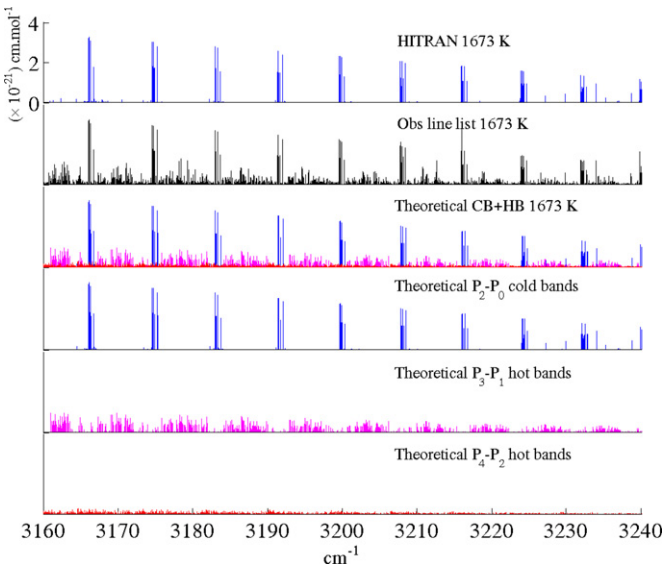

Figure 5. Comparison for the stick spectrum of a portion of the pentad between theoretical (this work), experimental (Hargreaves et al. 2012, 2013), and HITRAN2008 line lists at 1673 K. The CB+HB decomposition is also given.

(A color version of this figure is available in the online journal.)

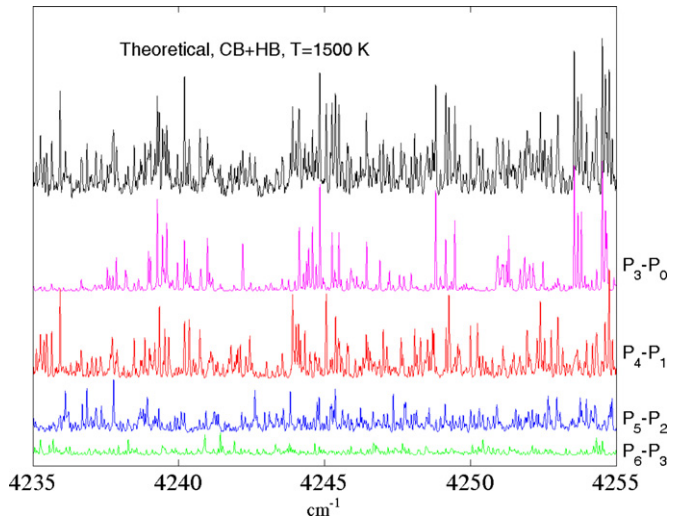

Figure 6. Detailed portion of the theoretical line list at 2.35 μm and CB+HB decomposition at 1500 K. The absorption spectra were simulated with a line profile at a resolution of 0.01 cm^{-1}.

(A color version of this figure is available in the online journal.)

convergence of variational calculations with the basis set size is more reliable for these lists. On the other hand, they are of a manageable size and include much fewer transitions by two orders of magnitude. The light lists contain additional fields for $J_{\rm low}$ and $J_{\rm up}$.

5. COMPARISON WITH EXISTING DATABASES

5.1. Experimental High-resolution Line Lists

Before checking the validity of the present lists with respect to high-T experimental spectra, we first consider the accuracy of our calculations via a benchmark comparison with the HITRAN database. To estimate the reliability of our variational calculations, we have computed the rms errors between

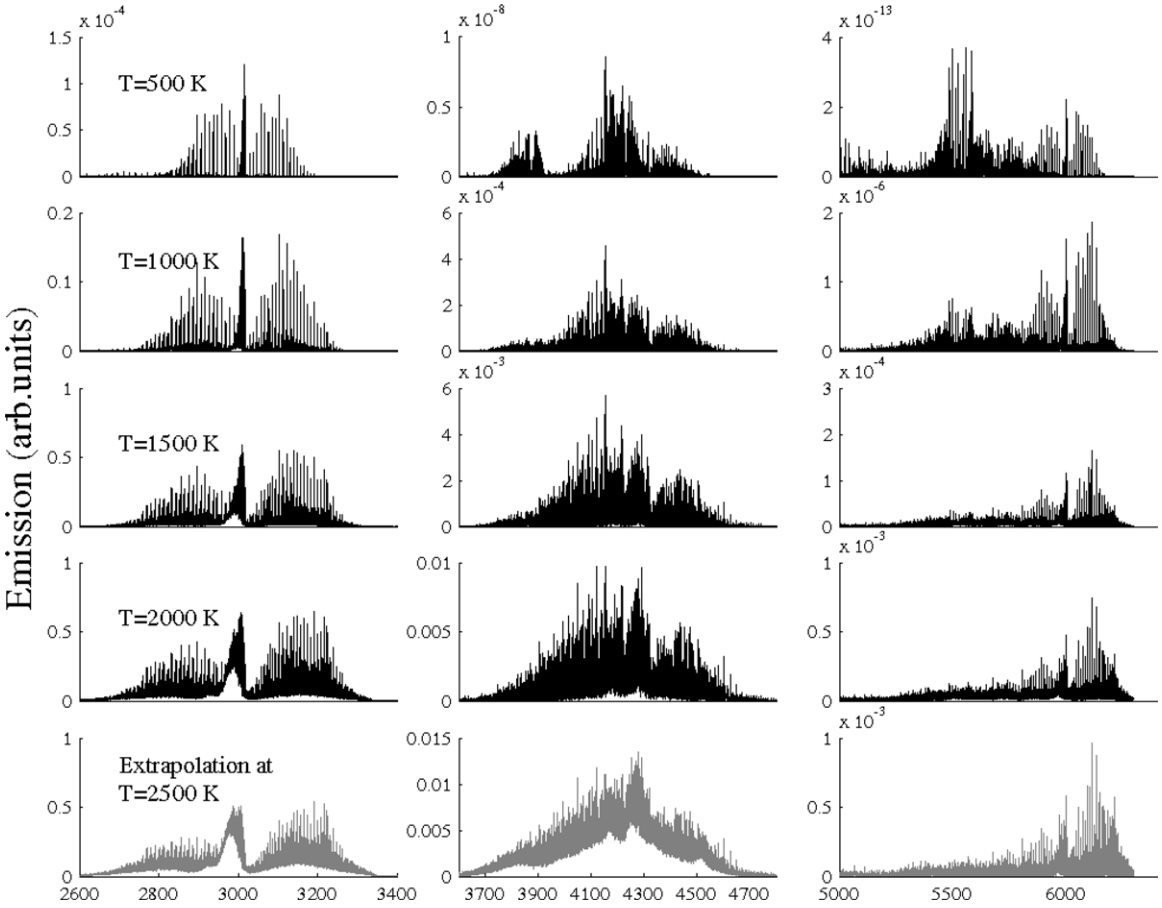

Figure 7. Emission spectra calculated from our theoretical line lists at a resolution of 0.01 cm^{-1} and a pressure of 0.02 torr. The three bottom panels (gray) are extrapolations to 2500 K from the 2000 K line list.

HITRAN lines and matching lines extracted from our $T = 296$ K list at various intensity cutoffs. These latter correspond to the same rovibrational quantum numbers, lower state energy levels, and symmetry labels as those given in HITRAN. To avoid ambiguities, the transitions with doubtful identification, which may appear for lines with very close frequencies, have been removed. We can see in Table 3 that errors for CB and HB are both below 0.1 cm^{-1} for positions and 5% for intensities, even for weak transitions. All these results thus suggest that our calculations approach spectroscopic accuracy, in a sense that the theoretical predictions could serve to assign some experimental spectral portions, at least at $T = 296$ K and for low-J values.

As a next step, we considered a comparison of our lists from $T = 500$ K to $T = 2000$ K with data extrapolated from HITRAN at the same temperatures. These comparisons are summarized in Table 4 and clearly provide evidence that a simple scaling of HITRAN from $T_{\rm room}$ to high temperatures should fail correctly describing hot spectra. This is mainly explained by the absence of the HB transitions. We see in Table 4 that HITRAN is composed essentially of CBs whose intensities are in good agreement with our results. The slightly underestimated P_i–P_0 values in HITRAN with increasing T could be explained by the absence of transitions for $J > 25$ in the database. To conclude with this table, it is worth noting that 17%, 52%, 81%, and 91% of the information contained in HBs at 500, 1000, 1500, and 2000 K, respectively, are missed in HITRAN2008 whereas the HITRAN2012 version contains some unreliable HB extrapolations which are not based on observed data. This is also corroborated by Figure 1, where lower state energies $E_{\rm low}^{\rm theo}$ and $E_{\rm low}^{\rm HITRAN}$ are plotted at 1000 and 2000 K. In order to study the impact of the HBs over a wider spectral range, we have plotted $E_{\rm low}$ for $\nu \in [1000, 10000]$ cm^{-1}. Note that appropriate $I_{\rm cutoff}$ were applied to avoid overloaded figures.

Further comparisons given in Figures 4–6 involve hot methane spectra measurements by Hargreaves et al. (Hargreaves et al. 2012, 2013). For this purpose, we use HBMIB experimental line lists produced at various temperatures from 300°C to 1400°C. Comparisons of the line integrated absorption cross sections at 1673 K between the theoretical (this work) and HBMIB are shown in Figure 4 for the dyad and the pentad. Our results are in excellent agreement with the HBMIB line list composed by measured and HITRAN lines.

Unlike the experimental list, our database is complete in the sense that we provide all $E_{\rm low}$ values. Consequently, we are able to compute absorption or emission spectra at an arbitrary temperature. Figure 5 displays a detailed portion of the 3 μm region and shows good agreement between the theoretical and experimental line lists. The CB+HB decomposition is also specified. As stated above, some parts of the HITRAN database only consist of CB transitions (see the top panel of Figure 5). Similarly, Figure 6 shows a detailed portion of the 2.35 μm region calculated from our theoretical database. As already seen in Table 4, the HBs are predominant for $T \gg T_{\rm room}$ and are thus essential for a complete characterization of hot spectra. In Figure 7, we illustrate predicted temperature effects in emission spectra. For that, we have converted the integrated absorption cross sections to emission spectra that are directly related to the

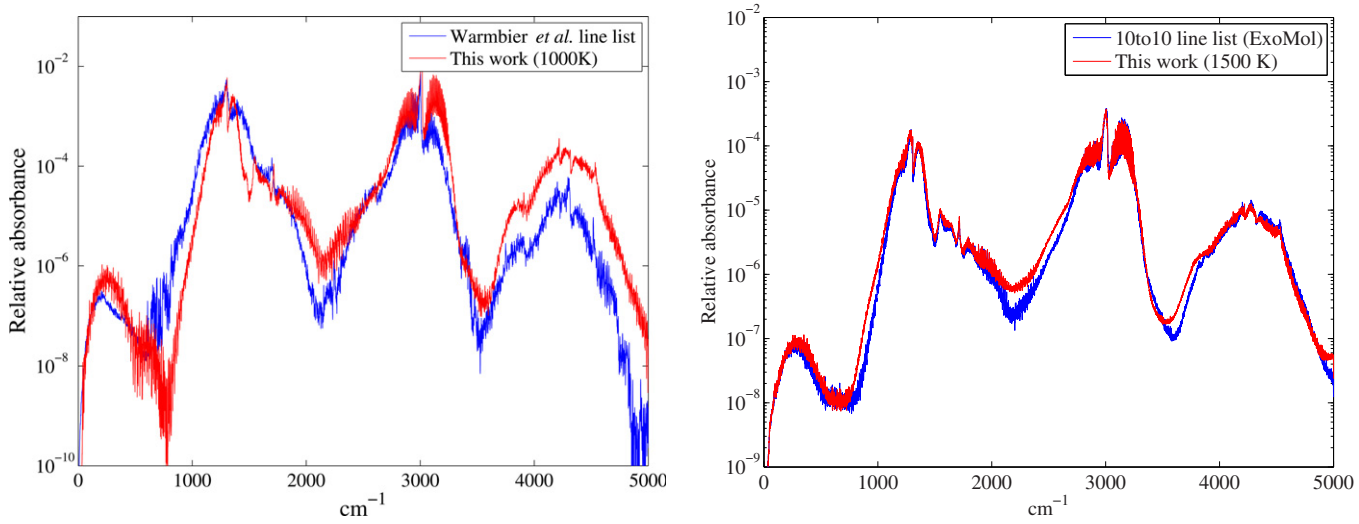

Figure 8. Relative absorption spectra simulated at the resolution of 0.5 cm^{-1} from our 1000 K line list (in red) compared to Warmbier et al. (2009) (in blue; left panel) and from our 1500 K line list (in red) compared to the 10-to-10 list from ExoMol (in blue; right panel).

(A color version of this figure is available in the online journal.)

observed properties of hot stellar objects. Additionally, to the four line lists, extrapolated spectra from 2000 to 2500 K are also given, but should be considered only as a simple qualitative illustration. Note that quantitative predictions for $T > 2000$ K could require including energy level calculations larger than our cutoff in J_{max} and $E_{low,max}$.

5.2. Theoretical Line Lists

We first compared our predictions with the theoretical line list of Warmbier et al. (2009) built at $T = 1000$ K. As the latter one had been not designed for high-resolution applications, we give here only a low-resolution overview comparison in the range of 0–5000 cm^{-1}. As is seen in Figure 8 in log scale, the qualitative features in absorption at this temperature are globally confirmed though there are quantitative deviations in certain ranges that could reach an order of magnitude. Above 2000 cm^{-1}, the calculations by Warmbier et al. (2009) are systematically underestimated with respect to our results in particular in transparency windows and in the octad range. This could be explained by the difference in the energy cutoff E_{low} in the two following calculations: 6000 cm^{-1} in their case and 14,000 cm^{-1} in ours. Many HB transitions are thus missing in their list.

After the submission of the first version of this paper, we became aware of the recent ExoMol variationally computed 10 to 10 list (Yurchenko & Tennyson 2014) built up to 1500 K and currently in press. This list is a very important step forward compared to previous available ones and covers a wide spectral range up to 1 μm. It includes all transitions up to $J = 39$ and for lower state energies E_{low}, up to 8000 cm^{-1}. For high-T calculations and also as noted by Yurchenko and Tennyson, this energy cutoff turns out too drastic to fully account for all significant HB transitions. Our cutoff is considerably higher with $J_{max} = 50$ and E_{low} up to 14,000 cm^{-1}. For this reason, we have many more transitions which contribute to the methane opacity in the range of 0–5000 cm^{-1} at $T = 1500$ K when applying the same intensity cutoff. When extrapolating the $T = 1500$ K ExoMol list (Yurchenko & Tennyson 2014) to 2000 K, the difference would be even more pronounced. A comparison of the number of transitions is added in the last column of the revised version of Table 4. A preliminary comparison of the theoretical lists gives quite good global agreement at a bird's eye view, at least up to $T = 1000$ K. Individual lines do not match exactly because different PES and DMS were used and also because computational methods employed do not have the same convergence properties. At $T = 1500$ K, our line list gives about ~15% more opacity, especially in the inter-polyad ranges (see Figure 8). This would be amplified if extrapolated to 2000 K with ~30% of difference.

6. CONCLUSION

The present work aims at providing, for the first time, a global theoretical line list for methane up to $T = 2000$ K. In the considered wavenumber range 0–5000 cm^{-1}, our theoretical lists are also the most complete for $T = 1000$ and 1500 K as they correspond to the highest cutoff in lower state energies and in J quantum numbers. Comparisons with laboratory observations (see Figures 4–6) show that for lower temperatures, the accuracy of predicted line positions and intensities are improved with respect to previous works. Theoretical ab initio predictions can be considered as a bridge between the "cold" spectroscopic HITRAN database and "hot" theoretical/experimental line lists, bringing complementary/supplementary information by adding much more data on HB transitions. It is well known that experimental line intensity measurements for HBs are quite laborious and delicate for crowded spectra involving impurities and a tremendous number of weak lines, many of them being blended. This requires precise knowledge of the temperature distribution and of other macroscopic parameters which are difficult to control. An accurate experimental measurement of a complete set of millions of line intensities under various temperature and pressure conditions is clearly beyond practical feasibility. Interchange of information between theory and experiment is of crucial importance in this domain. For example, preliminary comparisons of our calculations with the first version of the HBMIB list have allowed suggesting some modifications in extrapolated values which were fixed in the final version (Hargreaves et al. 2013). On the other hand, experimental validations are absolutely necessary to confirm the reliability of predictions. On the basis of various Obs.–Calc. comparisons, we estimate the uncertainty in integrated P_i–$P_{i'}$ intensities as about 3%, on average, for $\Delta i = 0$ and ~5% for

$\Delta i = 1$, whereas average uncertainties for line positions are expected to be of 0.1–1 cm^{-1} for low- and medium-J values. For higher Δi and J values and for individual line intensities, the errors could, of course, increase, particularly for weak transitions, but systematic measurements for corresponding quantum numbers are still missing.

A modeling of methane absorption and emission properties is a key issue for planetological and astrophysical applications. By neglecting a large number of transitions—which are not yet extracted from laboratory spectra analyses—this could lead to false conclusions in partial pressure profiles or in IR transparency windows observed, for instance, in methane-rich exoplanets or cool stars. Though the knowledge of all spectroscopic properties of hot methane is far from being perfect and still requires many experimental and theoretical efforts, the present line lists are steps toward a better characterization of the information missing in available databases. Our final 2000 K line list contains 11.5 billion lines, which are essential for a correct estimation of the opacity. Note that extended high-resolution spectroscopic data will be necessary for the interpretation of future exoplanet observations using new planned field spectrometers and space mission instruments with the resolving power improved by one or two orders of magnitude up to 20,000 (Tinetti et al. 2013).

To conclude, empirical corrections to the theoretical line lists could be introduced following the procedure recently applied for methane CBs (Tyuterev et al. 2013). Extension of the wavenumber range up to 12,000 cm^{-1} is currently in progress; the numerical convergence of calculations for higher polyads being under study. Full line lists are freely available at http://vamdc.univ-reims.fr/nas/.

Support for this work was provided by the IDRIS computer center of CNRS, the CINES computer center of France, as well as the Romeo computer center Reims-Champagne-Ardenne. This work has been partly supported by the French–Russian collaboration project SAMIA, by the methane project of French "Programme National de la Planetologie," by the visiting program of Reims University, as well as by the Tomsk State University Competitiveness Improvement Program. The authors thank R. Hargreaves and P. Bernath for providing us with their experimental line lists. Stimulating discussions with A. Coustenis, V. Boudon, R. Georges, and P. Lavvas are also acknowledged. The authors thank the reviewer for very valuable comments and suggestions for extending the intensity cutoff to include very weak lines.

REFERENCES

Albert, S., Bauerecker, S., Boudon, V., et al. 2009, CP, 356, 131
Ba, Y. A., Wenger, C., Surleau, R., et al. 2013, JQSRT, 130, 62
Barber, R. J., Tennyson, J., Harris, G. J., & Tolchenov, R. N. 2006, MNRAS, 368, 1087
Beaulieu, J.-P., Tinetti, G., Kipping, D. M., et al. 2011, ApJ, 731, 16
Borysov, A., Champion, J.-P., Jorgensen, U. G., & Wenger, C. 2002, MolPh, 100, 22
Boudon, V., Champion, J.-P., Gabard, T., et al. 2004, JMoSp, 228, 620
Brown, L. R., Sung, K., Benner, D. C., et al. 2013, JQSRT, 130, 201
Campargue, A., Leshchishina, O., Wang, L., et al. 2013, JMoSp, 291, 16
Cassam-Chenai, P., & Liévin, J. 2012, JChPh, 136, 174309
Champion, J.-P. 1977, CaJPh, 55, 1802
Coustenis, A., Iro, N., Moutou, C., Mayor, M., & Queloz, D. 2006, in Proc. IAUC200 Colloquium: Direct Imaging of Exoplanets: Science and Techniques, ed. C. Aimand & F. Vakili, Nice, France, 3–7 October (Cambridge: Cambridge Univ. Press), 171
de Bergh, C., Courtin, R., Bézard, B., et al. 2012, P&SS, 68, 85
Hargreaves, R. J., Beale, C. A., Michaux, L., Irfan, M., & Bernath, P. F. 2012, ApJ, 757, 46
Hargreaves, R. J., Beale, C. A., Michaux, L., Irfan, M., & Bernath, P. F. 2013, ApJ, 774, 89
Hirtzig, M., Bézard, B., Lellouch, E., et al. 2013, Icar, 226, 470
Huang, X., Schwenke, D. W., & Lee, T. J. 2011, JChPh, 134, 044320
Legget, S. K., Marley, M. S., Freedmann, R., et al. 2007, ApJ, 667, 537
Moses, J. I., Visscher, C., Fortney, J. J., et al. 2011, ApJ, 737, 15
Nakajima, T., Oppenheimer, B. R., Kulkami, S. R., et al. 1995, Natur, 378, 463
Nakajima, T., Tsuji, T., & Yanagisawa, K. 2001, ApJL, 561, L119
Nassar, R., & Bernath, P. 2003, JQSRT, 82, 279
Nikitin, A. V., Boudon, V., Wenger, Ch., et al. 2013a, PCCP, 15, 10071
Nikitin, A. V., Daumont, L., Thomas, X., et al. 2011a, JMoSp, 268, 93
Nikitin, A. V., Rey, M., Champion, J.-P., & Tyuterev, Vl. G. 2012, JQSRT, 113, 1034
Nikitin, A. V., Rey, M., & Tyuterev, Vl. G. 2011b, CPL, 501, 179
Nikitin, A. V., Rey, M., & Tyuterev, Vl. G. 2013b, CPL, 565, 5
Nikitin, A. V., Thomas, X., Régalia, L., et al. 2011c, JQSRT, 112, 28
Nixon, C. A., Temelso, B., Vinatier, S., et al. 2012, ApJ, 749, 159
Noll, K. S., Geballe, T. R., Leggett, S. K., & Marley, M. S. 2000, ApJL, 541, L75
Oppenheimer, B. R., Kulkarni, S. R., Matthews, K., & Nakajima, T. 1995, Sci, 270, 1478
Partridge, H., & Schwenke, D. W. 1997, JChPh, 106, 4618
Rey, M., Nikitin, A. V., & Tyuterev, Vl. G. 2012, JChPh, 136, 24106
Rey, M., Nikitin, A. V., & Tyuterev, Vl. G. 2013a, PCCP, 15, 10049
Rey, M., Nikitin, A. V., & Tyuterev, Vl. G. 2013b, JMoSp, 291, 85
Rothman, L. S., Gordon, I. E., Babikov, Y., et al. 2013, JQSRT, 130, 4
Rothman, L. S., Gordon, I. E., Barbe, A., et al. 2009, JQSRT, 110, 533
Rothman, L. S., Gordon, I. E., Barber, R. J., et al. 2010, JQSRT, 111, 2139
Schwenke, D., & Partridge, H. 2001, AcSpA, 57, 887
Swain, M. R., Deroo, P., Griffith, C. A., et al. 2010, Natur, 463, 637
Swain, M. S., Vasisht, G., & Tinetti, G. 2008, Natur, 452, 329
Swain, M. S., Vasisht, G., Tinetti, G., et al. 2009, ApJL, 690, L114
Tennyson, J., & Yurchenko, S. N. 2012, MNRAS, 425, 21
Thiévin, J., Georges, R., Carles, S., et al. 2008, JQSRT, 109, 2027
Tinetti, G., Coustenis, A., & Encrenaz, Th. 2013, A&A, 21, 63
Tinetti, G., Liang, M.-C., Vidal Madjar, A., et al. 2007a, ApJL, 654, L99
Tinetti, G., Vidal Madjar, A., Liang, D., et al. 2007b, Natur, 448, 169
Tyuterev, Vl. G., Tashkun, S., Rey, M., et al. 2013, JPCA, 117, 13779
Wang, X.-G., & Carrington, T., Jr. 2003, JChPh, 119, 101
Warmbier, R., Scheider, R., Sharma, A. R., et al. 2009, A&A, 495, 665
Wenger, C., Champion, J.-P., & Boudon, V. 2008, JQSRT, 109, 2687
Yurchenko, S. N., Barber, R. J., & Tennyson, J. 2011, MNRAS, 413, 1828
Yurchenko, S. N., & Tennyson, J. 2014, MNRAS, in press (arXiv:1401.4852)
Yurchenko, S. N., Tennyson, J., Barber, R. J., & Thiel, W. 2013, JMoSp, 291, 69